



International Journal of Intellectual Advancements and Research in Engineering Computations

Detection of land cover change using fuzzy segmentation algorithm

M.Ramya, R.Ramya, K.Sangeetha, V.Prakash, Dr. N.S.Nithya, Dr.E.Baby Anitha

Department of Computer Science and Engineering K.S.R College of Engineering (Tiruchencode)

ABSTRACT

Detection of Land cover changes like forest DETECTION OF LAND COVER CHANGE USING FUZZY SEGMENTATION ALGORITHM Department fire, flood and cultivation is the important criterion for farmers. This paper proposes a Land cover detection model using Fuzzy Local C-Mean clustering model (FLC-C). Fuzzy Local C-Mean clustering model method is implemented to process subsequences of time series data and detects land cover change temperature measured as a function of time. Land surface temperature is measured and declared when consecutive subsequences that are extracted from one Moderate Resolution Imaging Spectroradiometer (MODIS) time series transitions from one cluster to another cluster and remains in the newly assigned cluster for the rest of the time series. The temporal sliding window designed to operate on a subsequence of the time series to extract information from two spectral bands from the MODIS product.

Keywords: Land Cover Change, MODIS, Image Segmentation. Fuzzy Segmentation, Fuzzy Local C-Mean Clustering

INTRODUCTION

Digital image processing is the use of computer algorithms to perform image processing on digital images. As a subcategory or field of digital signal processing, digital image processing has many advantages over analog image processing. It allows a much wider range of algorithms to be applied to the input data and can avoid problems such as the build-up of noise and signal distortion during processing. Since images are defined over two dimensions (perhaps more) digital image processing may be modeled in the form of multidimensional systems.

Image segmentation is the process of partitioning a digital image into multiple segments (sets of pixels, also known as super-pixels). The goal of segmentation is to simplify and/or change the representation of an image into something that is more meaningful and easier to analyze. Image segmentation is typically used to locate objects and boundaries (lines, curves, etc.) in images. More precisely, image segmentation is the process of assigning a label to every pixel in an image such

that pixels with the same label share certain characteristics. The transformation of natural vegetation by practices such as deforestation, agricultural expansion, urbanization and natural disasters such as forest fires and floods has significant impacts on hydrology, ecosystems and climate. Coarse spatial resolution satellite data provide the regional, spatial, long-term and high temporal measurements for monitoring the earth surface.

Automated land cover change detection at regional or global scales, using hyper-temporal, coarse resolution satellite data has been a highly desired but elusive goal of environmental remote sensing. Hence, this project provides an automated land cover change detection method that uses coarse spatial resolution hyper-temporal earth observation satellite time series data. In addition, the details such as wild life movement, forest fire, deforestation and changes in vegetation nature are also covered. Based on the images collected at regular intervals, the comparison are made and analyzed. Using feature extraction process that creates meaningful sequential time series that can

Author for correspondence:

Department of Computer Science and Engineering K.S.R College of Engineering (Tiruchencode)

be analyzed and processed for change detection. In addition, the Fuzzy C-Means approach is used to cluster the various types of sub image details. The method was evaluated on real and simulated land cover change examples and obtained more change detection accuracy.

LITERATURE SURVEY

J. Hansen et al [1] describe the Goddard Institute for Space Studies (GISS) analysis of global surface temperature change, compare alternative analyses, and address questions about perception and reality of global warming. Satellite-observed nightlights are used to identify measurement stations located in extreme darkness and adjust temperature trends of urban and peri-urban stations for non-climatic factors, verifying that urban effects on analyzed global change are small. Because the GISS analysis combines available sea surface temperature records with meteorological station measurements, we test alternative choices for the ocean data, showing that global temperature change is sensitive to estimated temperature change in polar regions where observations are limited.

Felix N. Kogan et al [2] describe the main goal of global agriculture and the grain sector is to feed 6 billion people. Frequent droughts causing grain shortages, economic disturbances, famine, and losses of life limit the ability to fulfill this goal. To mitigate drought consequences requires a sound early warning system. The National Oceanic and Atmospheric Administration (NOAA) has recently developed a new numerical method of drought detection and impact assessment from the NOAA operational environmental satellites. The method was tested during the past eight years, adjusted based on users' responses, validated against conventional data in 20 countries, including all major agricultural producers, and was accepted as a tool for the diagnosis of grain production. Now, drought can be detected 4–6 weeks earlier than before, outlined more accurately, and the impact on grain reduction can be predicted long in advance of harvest, which is most vital for global food security and trade. This paper addresses all these issues and also discusses ENSO impacts on agriculture.

Jose A. Sobrino et al [3] describe a SPECTRA (Surface Processes and Ecosystem Changes Through Response Analysis) is one of the core candidate missions which is being proposed for implementation in the European Space Agency (ESA) Earth Explorer program of research oriented missions. The scientific objective of the SPECTRA mission is to describe, understand, and model the role of terrestrial vegetation in the global carbon cycle and its response to climate variability under the increasing pressure of human activity. The SPECTRA satellite will embark an optical hyperspectral payload covering the solar spectral range (0.4 to 2.4 μm) and thermal infrared region (10.3 to 12.3 μm). This paper is focused on the land surface temperature retrieval from SPECTRA thermal infrared data. In the first part of the paper, generalized single-channel and split-window methods are discussed and compared, showing that single-channel methods provide similar or better results than split-window methods for low atmospheric water vapor content, whereas split-window methods always provide better results for high atmospheric water vapor content. In the second part of the paper, split-window and dual-angle algorithms have been developed for SPECTRA thermal channels.

Zhengming Wan et al [4] describe about a generalized split-window method for retrieving land Cover Change from AVHRR and MODIS data. Accurate radiative transfer simulations show that the coefficients in the split-window algorithm for Land Cover Change must vary with the viewing angle, if we are to achieve a Land Cover Change accuracy of about 1 K for the whole scan swath range (USE'from nadir) and for the ranges of surface temperature and atmospheric conditions over land, which are much wider than those over oceans. We obtain these coefficients from regression analysis of radiative transfer simulations, and we analyze sensitivity and error over wide ranges of surface temperature and emissivity and atmospheric water vapor abundance and temperature. Sim- ulations show that when atmospheric water vapor increases and viewing angle is larger than 45', it is necessary to optimize the split-window method by separating the ranges of the at- mospheric water vapor, lower

boundary temperature, and the surface temperature into tractable subranges.

Juan C. Jimenez-Munoz et al [5] describe a algorithms to retrieve land surface temperature from at-sensor and land surface emissivity data. These algorithms have been specified for different thermal sensors on board satellites, i.e., the algorithm used for one thermal sensor (or a combination of thermal sensors) cannot be used for other thermal sensor. The main goal of this paper is to propose a generalized single-channel algorithm that only uses the total atmospheric water vapour content and the channel effective wavelength (assuming that emissivity is known), and can be applied to thermal sensors characterized with a FWHM (Full-Width Half-Maximum) of around 1 mm actually operative on board satellites. The main advantage of this algorithm compared with the other single channel methods is that in-situ radiosoundings or effective mean atmospheric temperature values are not needed, whereas the main advantage of this algorithm compared with split-window and dual-angle methods is that it can be applied to different thermal sensors using the same equation and coefficients

METHODOLOGIES

Thermal emissivity ϵ is the efficiency with which a surface emits the stored heat as thermal infrared (TIR) radiation. It is useful to indicates the composition of the radiating surface and necessary as a control in atmospheric and energy-balance models, since it must be known along with brightness temperature to establish the heat content of the surface. The first practical demonstration of multispectral TIR imaging for compositional mapping was from a NASA airborne scanner flown over Utah. Emissivity differs from wavelength to wavelength, just as reflectivity r does in the spectral region of reflected sunlight (0.4–2.5 mm). Emissivity is defined as

$$\epsilon(\lambda) = \frac{L(\lambda, T)}{B(\lambda, T)}$$

Where L is the measured spectral radiance and B is the theoretical blackbody spectral radiance for a surface with a skin temperature T . B is given by Planck's law which, together with the basic physics of TIR radiative transfer, is discussed in the entry Land Cover Change. Unlike T , which is a variable property of a surface controlled by the heating history and not directly by composition, $\epsilon(\lambda)$ is independent of Land is a function directly of composition. Furthermore, $\epsilon(\lambda)$ in the TIR wavelengths (3–14 mm) responds to different aspects of composition than reflectivity $r(\lambda)$ at 0.4–2.5 mm. In general, r at wavelengths 0.4–2.5 mm is controlled by the amounts of iron oxides, chlorophyll, and water on the surface; ϵ in the TIR is controlled more by the bond length of Si and O in silicate minerals.

TIR spectroscopy is especially important because silicate minerals are the building blocks of the geologic surface of Earth, and their presence and amounts can be inferred only indirectly at shorter wavelengths. Thus TIR spectroscopy is complementary to spectroscopy of reflected sunlight. Good summaries of TIR spectroscopy and its significance in terms of surface composition.

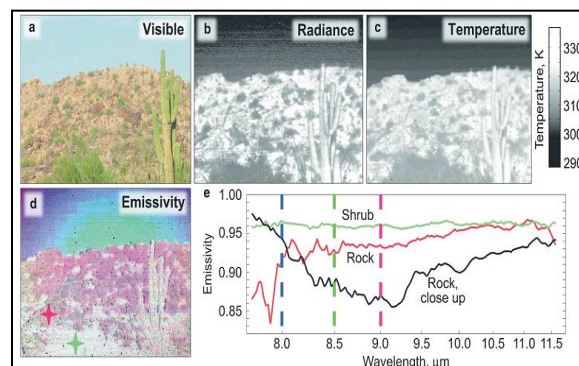
Daytime and nighttime false-color composite images of spectral radiance from a sparsely vegetated part of Death Valley, California, enhanced using a decor relation contrast stretch. This stretch emphasizes the emissivity component of the signal, shown as color, and de-emphasizes the temperature, shown as dark/light intensity. In addition to composition, the daytime image gives a good sense of topography, because sunlit slopes are warmer than shadowed slopes. In the nighttime image, most temperature effects are subdued, and the image closely resembles the Land Surface Emissivity (LSE) alone.

Exceptions include standing water, which is cooler than the land during the day but warmer at night. Standing water (C) in the floor of Death Valley shows dark green in the daytime image but light pink in the nighttime image. Vegetation (A) appears dark in the daytime image, when it is cooling its canopy by evapotranspiration. The toe of an alluvial fan (B) appears darker at night, when soil moisture rises to the surface and evaporates.

- **Land surface emissivity (LSE).** Average emissivity of an element of the surface of the Earth calculated from measured radiance and land surface temperature (LST).
- **Atmospheric window.** A spectral wavelength region in which the atmosphere is nearly transparent, separated by wavelengths at which atmospheric gases absorb radiation.
- **Blackbody.** An ideal material absorbing all incident energy or emitting all thermal energy possible. A cavity with a pinhole aperture approximates a blackbody.
- **Brightness temperature.** The temperature of a blackbody that would give the radiance measured for a surface.
- **Color temperature.** Temperature satisfying Planck's law for spectral radiances measured at two different wavelengths.
- **Contrast stretch.** Mathematical transform that adjusts the way in which acquired radiance data translate to the black/white dynamic range of the display monitor.
- **Emissivity ϵ .** The efficiency with which a surface radiates its thermal energy.
- **Irradiance.** The power incident on a unit area, integrated over all directions ($W m^2$).
- **Gray body.** A material having constant but non-unity emissivity.
- **Thermal infrared (TIR).** Thermal energy is radiated from a body at frequencies or wavelengths in proportion to its temperature. The wavelengths for which this radiant energy is significant for most terrestrial surfaces (1.4–14 mm) are longer than the wavelength of visible red light and hence are known as thermal infrared.
- The TIR is subdivided into three ranges (LWIR, MIR, SWIR) for which the atmosphere is transparent (atmospheric “windows”) so that the energy can be measured from space.

MIR IMAGE

In principle, this problem can be removed by increasing the number of images acquired for the same scene. For each n -channel image, after atmospheric compensation, there are $n + 1$ unknowns, but only n measurements; for two images of the same scene, there are $n + 2$ unknowns, but $2n$ measurements (assuming LST has changed but LSE has remained constant). Therefore, a two-channel image taken at two different times is deterministic. It is additionally necessary that the LST be significantly different between acquisitions.



Two-time, two-channel approach If well-registered multispectral day–night radiance measurements are available, it is possible to determine T and ϵ uniquely (Watson, 1992a). Although this approach is esthetic, for most TIR data, the recovered temperatures and emissivities tend to be imprecise. For example, for image channels at 8 and 12 mm, day–night temperatures

of 290 and 310 K, and for NEDT $\frac{1}{4}$ 0.3 K, recovered LST would have an uncertainty of 20 K. This arises because of the flat shape of the Planck curve in the spectral range around 300 K. By using an image channel in the 3–5 mm window, where the slope of the Planck function is steep, can improve the precision greatly and used the day–

night algorithm to make a standard MODIS LST product.

- Natural color.
- MIR radiance at 9 mm.
- Brightness temperature.
- Emissivity (RGB ¼ 8, 8.5 and 9 mm, respectively).
- Emissivity spectra measured with the TELOPS.

SPECTRAL-SHAPE SOLUTIONS

Although it is not possible to invert the modified Planck equation for both ϵ and T without external constraints, it is possible to estimate spectral shape for ϵ , at the expense of T and of the amplitude of the recovered spectrum, that is, the recovered spectra are essentially normalized, so that only relative amplitudes (wavelength to wavelength) are known. This is nevertheless useful, since composition is generally determined from spectral shape, and not the absolute amplitudes.

Observed that ratios of spectrally adjacent channels i and j described spectral shape accurately, provided that T could be estimated even roughly

$$\frac{\epsilon_j}{\epsilon_i} = \frac{L_j \lambda_i^5 (\exp(c_2/(\lambda_i T)) - 1)}{L_i \lambda_j^5 (\exp(c_2/(\lambda_j T)) - 1)}$$

To calculate the ϵ ratios, it is necessary to approximate the temperature T from the measured radiances L_i and L_j . If ϵ can be estimated with in 0.075, the uncertainty in T is 5 K, and the ϵ ratios can be estimated with an average error of 0.007 (this estimate does not include the effects of measurement error). Becker and Li (1990) proposed a similar approach they called the “temperature-independent spectral indices” (TISI) method. TISI begins with the observation (Slater, 1980) that Planck’s law may be represented by

$$B_k(T_s) = \alpha_k(T_o) T^{n_k(T_o)}$$

Where B is the spectral radiance in image channel k for a blackbody at temperature T_s and

T_o is a reference temperature. Constants n_k and α_k are given by

$$n_k(T_o) = \frac{c_2}{\lambda_k T_o} \left(1 + \frac{1}{\exp(c_2/\lambda_k T_o) - 1} \right);$$

$$\alpha_k(T_o) = \frac{B_k(T_o)}{T_o^{n_k(T_o)}}$$

The land-leaving spectral radiance L_k , corrected for atmospheric absorption and path radiance but not down-welling spectral irradiance L_k .

$$L_k = \epsilon_k \alpha_k T_s^{n_k} C_k; \quad C_k = 1 + \frac{(1 - \epsilon_k) L_s^{\downarrow}}{\epsilon_k B_k(T_s)}$$

Where C_k is spatially variable and atmosphere specific. The TISI is found by rationing spectral radiances for image channels i and j . Here a_i is defined as $n_i - 1$ (and $a_j = n_j - 1$), chosen to make Equation 6 independent of T . Since for a wide range of temperatures the C ratio is close to unity, TISI is then.

The ratio spectra are insensitive to temperature, for normal terrestrial ranges. The approaches are adaptable for most sensors

$$TISI_{i,j} = \left[\frac{L_i}{\alpha_i} \right]^{1/n_i} \left[\frac{L_j}{\alpha_j} \right]^{-1/n_j} = \frac{\epsilon_i^{1/n_i} C_i^{1/n_i}}{\epsilon_j^{1/n_j} C_j^{1/n_j}} \approx \frac{\epsilon_i^{1/n_i}}{\epsilon_j^{1/n_j}}$$

ALPHA-RESIDUAL METHOD

The alpha-residual algorithm produces a relative emissivity spectrum that preserves spectral shape but, like the ratio methods, does not yield actual ϵ or T values. The alpha residuals are calculated utilizing Wien’s approximation of Planck’s law, which neglects the “-1” term in the denominator. This makes it possible to linearize the approximation with logarithms, thereby separating λ and T

$$\frac{c_2}{T} \approx \lambda_j \ln(\varepsilon_j) - \lambda_j \ln(L_j) + \lambda_j \ln(c_1) - 5\lambda_j \ln(\lambda_j) - \lambda_j \ln(\pi).$$

Here c_1 and c_2 are the constants defined in Planck's law (Equation 1, Land Surface Temperature) and j is the image channel. Wien's approximation introduces a systematic error in ε_j of 1 % at 300 K and 10 mm wavelength. The next step is to calculate the means for the parameters of the linearized equation, summing over the n image channels:

$$\frac{c_2}{T} \approx \frac{1}{n} \sum_{j=1}^n \lambda_j \ln(\varepsilon_j) - \frac{5}{n} \sum_{j=1}^n \lambda_j \ln(\lambda_j) - \frac{1}{n} \sum_{j=1}^n \lambda_j \ln(L_j) + (\ln(c_1) - \ln(\pi)) \frac{1}{n} \sum_{j=1}^n \lambda_j.$$

The residual is calculated by subtracting the mean from the individual channel values. Collecting terms, a set of n equations is generated relating ε_i to L_i , independent of T .

Note that k_i contains only terms which do not include the measured spectral radiances, L_i , and hence may be calculated from the constants. Although dependency on T has been eliminated, it has been replaced by the unknown μ_α , related to the mean emissivity, such that the total number of unknowns is unchanged. The components of the alpha-residual spectrum vary only with the measured radiances. They are defined as

$$\alpha_i \equiv \lambda_i \ln(\varepsilon_i) - \mu_\alpha$$

Model approaches In this section, three algorithms distinguished by their model assumptions are described. The most specific requires that both a value of ε and the wavelength at which it occurs be known. The next requires only that the value be known. The third does not require the value of the emissivity to be known, only that the emissivity at two known wavelengths be the same. The model emissivity (or reference channel) method assumes that the value of ε for

one of the image channel's ref is constant and known a priori, reducing the number of unknowns to the number of measurements. First, the temperature is estimated using

$$T = \frac{c_2}{\lambda_{ref}} \left(\ln \left(\frac{c_1 \varepsilon_{ref}}{\pi L_{ref} \lambda_{ref}^5} \right) + 1 \right)^{-1}$$

Scaling approaches Once relative spectra have been calculated, they can be calibrated to "absolute" emissivity provided a scaling factor is known. Applied to the ratio approach of this is basically the same as one of the model algorithms. However, scaling can also be done from empirical regression relating the shape of the emissivity spectrum to an absolute value at one wavelength. The regression is typically based on laboratory spectra of common scene components. More complex approaches also are possible: the first example given below combines the "two-channel, two-time," and TISI approaches to convert the relative TISI spectra to emissivities.

The hybrid TISI approaches requires first that daytime and nighttime MIR and LWIR images be acquired and co-registered and that their TISI ratios be calculated. Essentially, there are four measurements (LMIR, day, LLWIR, day, LMIR, night, and LLWIR, night), four unknowns (ε_{MIR} , ε_{LWIR}), and one model assumption (the solar irradiance on the target). The MIR reflectivity is the complement of ε_{MIR} by Kirchhoff's law using widely separated image channels improves the precision of T and ε recovery.

ALPHA-DERIVED EMISSIVITY (ADE) METHOD

The key innovation of the ADE approach is to utilize the empirical relationship between the average ε and a measure of the spectral contrast or complexity in order to restore the amplitude to the alpha-residual spectrum. The regression is based on the observation that, for a blackbody, the mean emissivity is unity and the spectral variance is zero. For minerals with rest bands or other emissivity features, the variance is greater than

zero and, of course, the mean is less than unity. In use, the mean is predicted from the variance, which is calculated from the measured radiances

EXPERIMENTAL RESULTS

This table 5.1 shows the details of the image that is image taken from different locations or different area the size of the image in mega byte. The existing analysis and the proposed fuzzy automatic clustering are listed in this table.

Table 4.1 Area Wise Analysis

Area wise image	Size of image in MB	Existing analysis	Fast Fuzzy Local C-Mean Clustering
Water area	55	23	34
Land area	62	30	40
Agriculture area	74	42	50
Industrial area	82	52	63
Populated area	95	66	78

The Fig 5.1 shows that area wise analysis Land Cover Change Detection Model. The figure

describes the Size of Image and Average Analysis for Land Cover Detection Process.

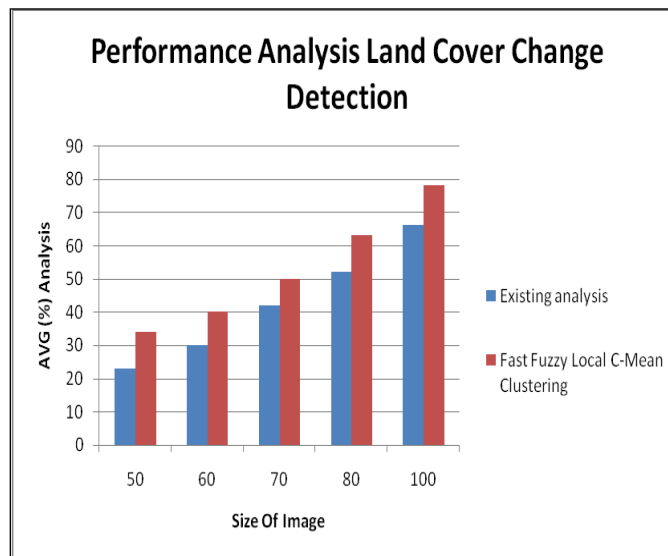


Fig 5.1 Area Wise Analysis

This table 5.2 shows the details of the image that is image taken from time to time that are represented in milliseconds. The existing analysis

and the proposed fuzzy automatic clustering are listed in this table with their time analysis.

Table 5.2 Land Cover Change Time Analysis

Area wise image	Size of image in MB	Existing analysis in m sec	Fast Fuzzy Local C-Mean Clustering in m sec
Water area	55	0.011	0.009

Land area	62	0.026	0.019
Agriculture area	74	0.035	0.022
Industrial area	82	0.046	0.036
Populated area	95	0.054	0.044

The Fig 5.2 shows that area wise analysis Land Cover Change Detection Time analysis Model. The

figure describes the Size of Image and Time Analysis for Land Cover Detection Process.

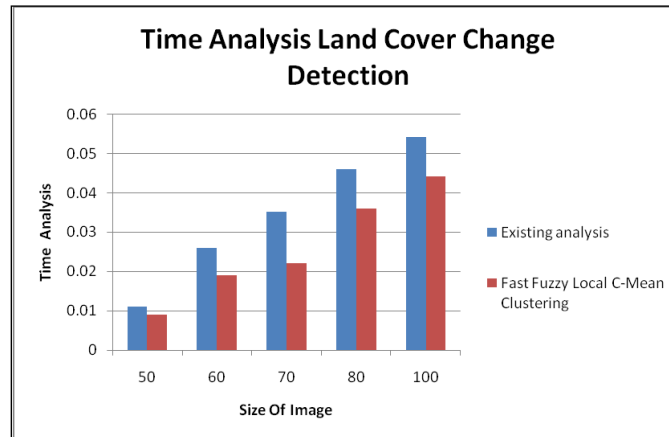


Fig 5.2 Land Cover Change Time Analysis

CONCLUSION

The proposed system concentrate in finding the specified area problem by using the MODIS image in that a region of the place is selected and that is separated as the land and the water area and the temperature is been noted. On the basis of radiative transfer theory in the MIR region, a bidirectional reflectivity retrieval method was used to separate the reflected solar direct irradiance and the radiances emitted by the surface and atmosphere. A kernel-driven model was proposed to describe the non-Lambertian reflective behavior

of the land surface and to accordingly determine the directional emissivity if there were more than three bidirectional reflectance available with different angular configurations on several consecutive days. The results showed that the bias and RMSE between the LSTs retrieved from MODIS daytime MRI data and those calculated using in situ measurements, at the time of the MODIS images. The proposed method could be used to accurately retrieve LST from MODIS daytime MIR data.

REFERENCES

- [1]. J. Hansen, R. Ruedy, M. Sato, and K. Lo, "Global surface temperature change," *Rev. Geophys.*, Art.no. RG4004, 48(4), 2010.
- [2]. F. N. Kogan, "Operational space technology for global vegetation assessment," *Bull. 3 Amer. Meteorol. Soc.*, 82(9), 2001, 1949–1964.
- [3]. J. A. Sobrino and J. C. Jiménez-Muñoz, "Land surface temperature retrieval from thermal infrared data: An assessment in the context of the surface processes and ecosystem changes through response analysis (SPECTRA) mission," *J. Geophys. Res.*, 110, 2005, D16, Art.no. D16103.
- [4]. Z. Wan and J. Dozier, "A generalized split-window algorithm for retrieving land-surface temperature from space," *IEEE Trans. Geosci. Remote Sens.*, 34(4), 1996, 892–905.

- [5]. J. C. Jiménez-Muñoz and J. A. Sobrino, “A generalized single-channel method for retrieving land surface temperature from remote sensing data,” *J. Geophys. Res.*, 8, D22, 2003, 4688–4695.
- [6]. B.-H. Tang et al., “Estimation and validation of land surface temperature from Chinese second generation polar-orbiting FY-3A VIRR data,” *Remote Sens.*, 7(3), 2015, 3250–3273.
- [7]. C. Gao, B.-H. Tang, H. Wu, X. Jiang, and Z.-L. Li, “A generalized split window algorithm for land surface temperature estimation from MSG-2/SEVIRI data,” *Int. J. Remote Sens.*, 34(12), 2013, 4182–4199.
- [8]. Berk et al., “MODTRAN cloud and multiple scattering upgrades with application to AVHRRIS,” *Remote Sens. Environ.*, 65(3), 1998, 367–375.
- [9]. Eduardo de Miguel, Elena Prado, Marcos Jiménez, Cristina Robles, “Evaluating the Information Content of the AHS MIR Bands”, *Proceedings 5th EARSeL Workshop on Imaging Spectroscopy*. Bruges, Belgium, 23-25, 2007.
- [10]. Alan Gillespie, “Land Surface Emissivity”, *Encyclopedia of Remote Sensing*, DOI 10.1007/978-0-387-36699-9, Springer Science+Business Media New York 2014.
- [11]. Lang Xia Kebiao Mao, Ying Ma, Fen Zhao, “An Algorithm for Retrieving Land Surface Temperatures Using VIIRS Data in Combination with Multi-Sensors”, *Sensors*; doi:10.3390/s141121385. 14, 2014, 21385-21408
- [12]. José A. Sobrino, Juan C et al, “Land Surface Emissivity Retrieval From Different VNIR and TIR Sensors”, *IEEE Transactions on Geo-Science and Remote Sensing*, 46(2), 2008.
- [13]. Li Fang, Yunyue Yu, Hui Xu, and Donglian Sun, “New Retrieval Algorithm for Deriving Land Surface Temperature from Geostationary Orbiting Satellite Observations”, *IEEE Transactions on Geo-Science and Remote Sensing*, 52(2), 2014.
- [14]. Xiaolei Yu, Xulin Guo and Zhaocong Wu, “Land Surface Temperature Retrieval from Landsat 8 TIRS—Comparison between Radiative Transfer Equation-Based Method, Split Window Algorithm and Single Channel Method”, *Remote Sens.* 6, 2014, 9829- 9852; doi:10.3390/rs6109829.
- [15]. Ying Sun, “Retrieval and Application of Land Surface Temperature”, - geo.utexas.edu ,Term Paper, 2011.
- [16]. Zhao-Liang Li, Ronglin Tang et al, “A Review of Current Methodologies for Regional Evapotranspiration Estimation from Remotely Sensed Data”, *Sensors* 9, 2009, 3801– 3853.
- [17]. J. Hansen, R. Ruedy, M. Sato, and K. Lo, “Global surface temperature change, ”*Rev. Geophys.*, Art. no. RG4004. 48(4), 2010.
- [18]. F. Sattari and M. Hashim, “A Brief Review of Land Surface Temperature Retrieval Methods from Thermal Satellite Sensors”, *Middle-East Journal of Scientific Research* 22 (5), 2014, 757-768.
- [19]. Zhengming Wan, “Validation and Refinement of the MODIS Land-Surface Temperature Product”, *MODIS Science Team Meeting*, 2011, 18-20.
- [20]. Guillem Sòria, José A. Sobrino, Mariam Atitar et al, “AATSR Land Surface Temperature Product: Comparison With SEVIRI and MODIS In The Framework Of CEFLES2 Campaigns”, *Proc. of the '2nd MERIS/ (A)ATSR User Workshop'*, Frascati, Italy 22–26, 2008.